FCC compliant 3.1-10.6 GHz UWB Pulse Radar System using Correlation Detection

J. Dederer, B. Schleicher, F. De Andrade Tabarani Santos, A. Trasser and H. Schumacher
Institute of Electron Devices and Circuits
University of Ulm,
89069 Ulm, Germany, Email: jochen.dederer@uni-ulm.de

***Abstract*— A short range 3.1 - 10.6 GHz single band ultra-wideband (UWB) pulse radar system is presented. The transmitter consists of a pulse generator that is connected to a broadband monopole antenna. The generated pulse shape is similar to the fifth derivative of the Gaussian bell shape and makes efficient use of the allocated FCC UWB frequency mask. The receiver is realized with a single-ended low noise amplifier and active single-ended to differential converters that drive the input ports of an analog correlator which uses pulse sequences as template signals. Measurements show a resolution capability of the radar system in the millimeter range. All active circuits have been realized in a low cost 0.8 μm SiGe HBT technology.**

***Index Terms*— UWB, pulse radar, SiGe HBT, impulse radio**

I. Introduction

UWB RF techniques offer well-recognized advantages for short range radar systems such as surface penetrating radars, medical imaging and sensing. Due to the broad bandwidth a high spatial resolution both in depth as in lateral dimensions is possible. Previous work on UWB radar systems includes the study of a superregenerative incoherent UWB pulse radar system [1] and an UWB InP-HEMT RF chipset for 24 GHz-band short range radar applications [2]. Digital UWB sensors using maximum length binary sequences as transmit signals with a corresponding bandwidth from nearly 0 to 5 GHz are described in [3]. Here we present a single band pulse radar system that is designed for operation in the allocated FCC UWB frequency band from 3.1 to 10.6 GHz [4]. The pulse-based radar system implements the original idea of UWB and allows simple low cost transceiver designs that make use of the inherent low complexity of such a system.

II. System architecture

A block diagram of the realized UWB radar system is given in Fig. 1. Two pulse generators provide continuous pulse trains on the transmit side (TX) as well as on the receiver side (RX) where the pulses are used as template signals for the correlation detection. The pulse generators are clocked by $\mathrm{CLK_{RX}}$ and $\mathrm{CLK_{TX}}$ with f_{RX} and f_{TX}, respectively, which can be varied from very low frequencies up to pulse repetition rates above 1 GHz. The pulse sequences are transmitted and

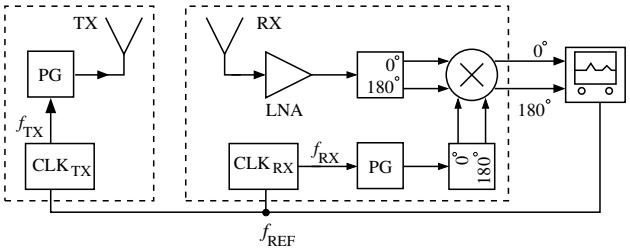

Fig. 1. Block diagram of the radar system with pulse generators (PG), antennas, LNA, baluns and analog correlator

received via two broadband monopole antennas. On the receiver side the incoming pulse sequence is amplified by a low noise amplifier that is followed by an analog correlator. The balanced input ports of the correlator are driven by two active single-ended to differential converter stages. The correlator core consists of a four-quadrant Gilbert cell multiplier. The differential output signal of the multiplier is low-pass filtered and further processed with a digital sampling scope. A common reference f_{REF} provides phase synchronisation for the measurement. In typical applications, a slight frequency offset is introduced between transmitter and receiver clocks. The frequency offset $\Delta f = f_{\mathrm{RX}} - f_{\mathrm{TX}}$ results in a periodically changing phase offset between the two signals. Periodic correlation peaks occur when a received pulse coincides with the template pulse. The exact position of the target is derived from the corresponding phase of the clock signal $\mathrm{CLK_{RX}}$ which depends on the time-of-arrival of the incoming pulses compared to a common reference.

III. MMIC chip set

All presented MMICs have been designed and fabricated using the commercially available 0.8 μm ATMEL SiGe2 HBT technology [5].

A. Pulse Generator

Pulse shapes usually found in literature are based on the Gaussian pulse and its derivatives. For indoor systems, at least the fifth-order derivative should be used to make most efficient use of the allocated spectrum mask [6]. Previously published proposals for integrated circuits that generate

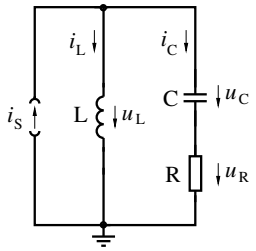

Fig. 2. Simplified schematic of monocycle pulse shaper

higher order derivatives are based on digital approaches that combine the output signals of several logic gates [7]. Here we present an efficient approach that is based on a R-L-C resonance circuit which is driven by a current pulse with a pulse shape similar to the Gaussian pulse. The currents in the R-L-C resonance circuit shown in Fig. 2 can be described by the following second-order differential equation

$$\frac{\mathrm{d}^2 i_\mathrm{C}}{\mathrm{d}\,t^2} + 2\,\delta\,\frac{\mathrm{d} i_\mathrm{C}}{\mathrm{d}\,t} + \omega_0^2\,i_\mathrm{C} = \frac{\mathrm{d}^2 i_\mathrm{S}}{\mathrm{d}\,t^2} \tag{1}$$

where the resulting impulse shape is determined by the damping parameter

$$\delta = \frac{R}{2\,L} \tag{2}$$

and the natural frequency

$$\omega_0 = \frac{1}{\sqrt{(LC)}}\ . \tag{3}$$

Setting the parameters of the resonance circuit to $C = 150\,\mathrm{fF}$, $L = 1.2\,\mathrm{nH}$ and $R = 50\,\Omega$ results in an under-damped response which is characterized by an exponentially decaying sinusoidal waveform. Stimulating this differentiating resonance circuit by a current pulse with a Gaussian bell shape of 83 ps fall width at half maximum leads to an output voltage u_R with a pulse shape similar to the fifth derivative of the Gaussian bell shape. The main difficulty here is to provide a current pulse with very short transition times as the pulse shape and the achievable pulse amplitude is determined by the risetime of the signal that controls the R-L-C resonance circuit. The short transition times are achieved by a two-stage limiting amplifier that is followed by a high-pass network that forms the controlling current pulse for the R-L-C pulse shaping network. The pulse amplitudes are adjustable to the emission limits set by the spectrum mask. A detailed description of this approach can be found in [8]. Fig. 3 shows the measured pulse shape of the mounted chip. Excellent agreement with the targeted pulse shape has been achieved. The spectrum of pulse sequences with regular pulse-to-pulse intervals shows discrete energy spikes corresponding to the repetitive period of consecutive pulses. The measured output spectrum of such a 200 MHz pulse train and its

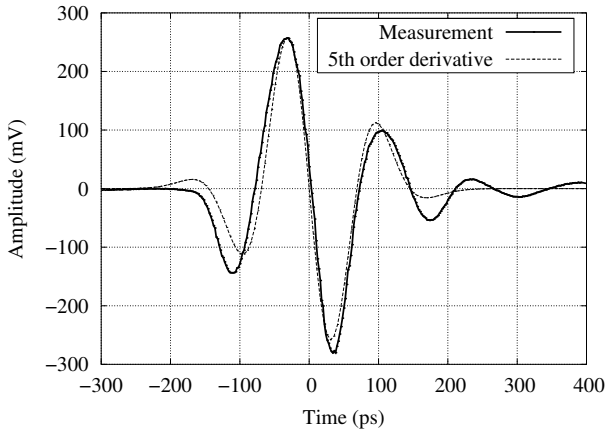

Fig. 3. Comparison of measured monocycle waveform with targeted 5th-order derivative monocycle scaled to the amplitude of the measured pulse

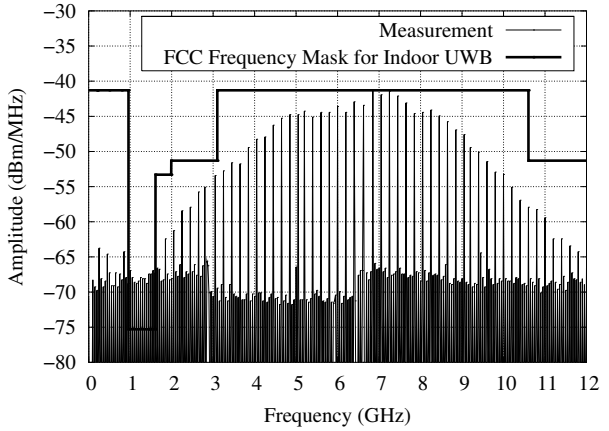

Fig. 4. Comparison of measured power spectral density with FCC regulatory mask for indoor UWB devices

compliance with the FCC regulatory spectrum mask for indoor UWB devices is depicted in Fig. 4. For this 200 MHz pulse train, the average power consumption of the mounted chip is 38 mW. The pulse generator is connected to a microstrip-fed monopole antenna which has been realized on a 0.508 mm Rogers RO4003C substrate. To achieve the maximum impedance bandwidth using a simple square monopole, a pair of notches is placed at the lower corners of the patch. The notch structure is embedded in a truncated ground plane. A detailed description of this approach can be found in [9].

B. Low Noise Amplifier

The LNA has been realized as a three-stage amplifier that uses a combination of local series feedback with capacitive emitter degeneration, local shunt feedback and global shunt feedback between the first and second stage to broaden the operating frequency range in terms of gain, linearity and noise matching. The complete chip,

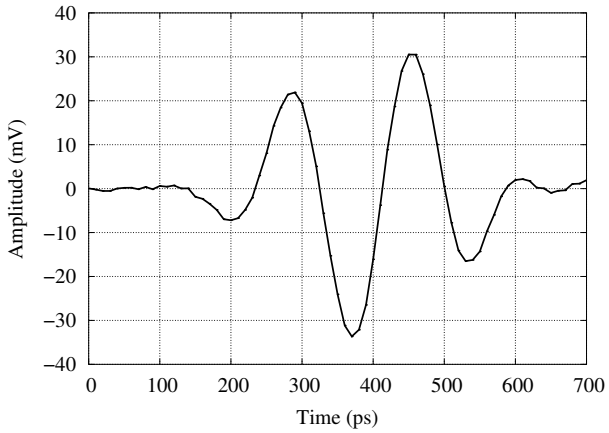

Fig. 5. Received pulse shape at LNA output

pads included, has a size of $0.17\,\mathrm{mm}^2$. The total power consumption of the LNA equals 55 mW. Detailed presentations of the LNA design and on-wafer performance characteristics can be found in [10]. Measurements of the received pulse shape were done in an anechoic chamber with the TX and RX antenna placed at a distance of 30 cm. The pulse shape at the output of the LNA is depicted in Fig. 5. Excellent pulse symmetry has been maintained.

C. Analog Correlator Core

Fig. 6 shows a simplified schematic of the UWB analog correlator core. The correlator core comprises a four-quadrant Gilbert cell multiplier with two active single-ended to differential converters at the input (RF) port and template signal (TS) port, respectively, a low-pass filter and a buffer amplifier stage. The Gilbert cell employs capacitively shunted emitter degeneration on the bottom differential pair. Shunt resistors at the RF and TS ports provide a broadband matching to the preceeding single-ended to differential converters. The differential outputs of the converters are taken at the collector and emitter node of a single transistor. Gain and phase accuracy is achieved with capacitively shunted emitter degeneration which compensates the load imbalance seen from the emitter and collector nodes, respectively. The differential output signal of the multiplier is fed into a pair of emitter followers and further processed with a digital sampling scope. The 800 MHz 3-dB multiplier output bandwidth is mainly determined by the corner frequency of the low-pass filter that is formed by the load resistors of the Gilbert cell together with the shunt capacitors at the input of the succeeding buffer stage. The lower cutoff frequency (3.5 GHz at - 3 dB) of the RF and TS inputs is set by the coupling capacitors between the single-ended to differential converters and the multiplier whereas the upper 3-dB cutoff frequency exceeds the UWB frequency band. Operated with sinusoidal inputs, the MMIC exhibits

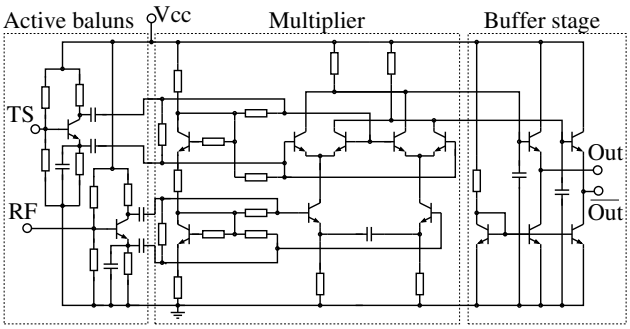

Fig. 6. Simplified schematic of wide-band analog correlator core with active baluns, multiplier and buffer stage

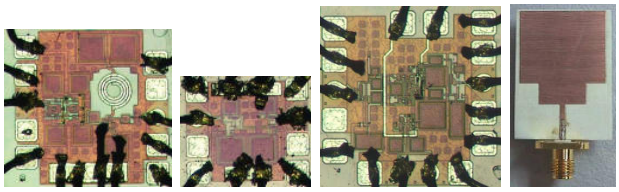

Fig. 7. Photographs of the mounted MMIC chip set and the monopole antenna

a single-ended conversion gain of $-4\,\mathrm{dB}$ and a 1 dB input compression point of $-1\,\mathrm{dBm}$ at the center of the UWB frequency band for an applied power of $-5\,\mathrm{dBm}$ to the TS port. Fed with pulses, the Gilbert cell acts as a true multiplier instead of switching the upper transistor quad as usually done in mixer applications. The power consumption of the multiplier together with the single-ended to differential converters equals 58 mW whereas the buffer stage draws 9 mA from the common 3 V supply. The complete chip, pads included, measures $0.33\,\mathrm{mm}^2$. Fig. 7 shows the mounted MMIC chip set and the monopole antenna.

IV. Experimental Results of the Pulse Radar System

The MMIC chipset was mounted in separate modules on a 0.305 mm Rogers RO4003C substrate. Additional 6 dB attenuators were placed between the LNA and the multiplier RF input and between the template generator and the TS input, respectively, to minimize multiple reflections. A $144\,\mathrm{cm}^2$ metal plate was used as the target object. To allow an easy assessment of the target distance, the antennas and the target were placed in a collinear arrangement where the RX antenna was positioned 15 cm to the right of the TX antenna and the target 10 cm to the left. The clock signals on the RX as well as on the TX side were set to a common frequency of 200 MHz. Depending on the time of arrival of the incoming pulses, the $\mathrm{CLK}_{\mathrm{RX}}$ phase was swept in one-degree-steps until a maximum cross-correlation energy was detected. Fig. 8

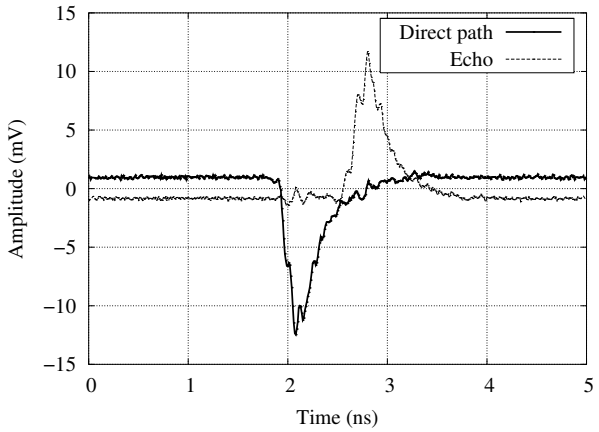

Fig. 8. Correlator core output signals for multiplication of time-aligned template pulse with received pulse from indirect path (echo) and received pulse from the direct path

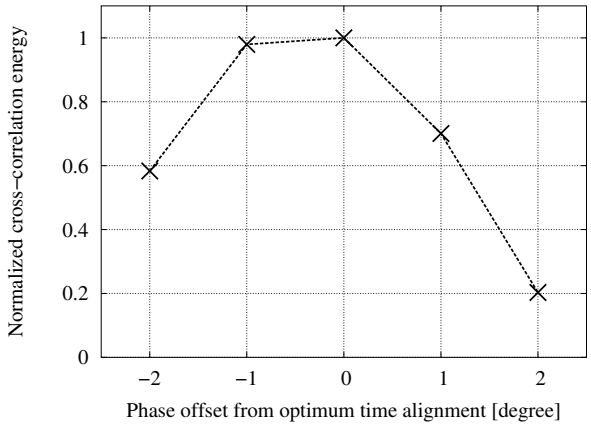

Fig. 9. Normalized cross-correlation energy of incoming pulse with template pulse

shows the AC-coupled output signals of the correlator core. The positive output signal in Fig. 8 results from the multiplication of a time-aligned template pulse with a reflected, phase-inverted pulse from the target whereas the negative peak corresponds to the multiplication of a time-aligned template pulse with a received pulse from the direct path between the TX and RX antenna. For simplicity reasons, we use the phase offset $\Delta\phi_{\mathrm{RX}}$ of the $\mathrm{CLK_{RX}}$ signals that have been time-aligned to the received pulses from the direct and indirect path, respectively, for the calculation of the spatial distance of the target. One degree of phase difference $\Delta\phi_{\mathrm{RX}}$ for a given pulse repetition rate of 200 MHz is equivalent to a time difference $\Delta\mathrm{t}$ of

$$\Delta\mathrm{t} = \frac{1}{200\,\mathrm{MHz}\cdot 360^\circ} \approx 13.9\,\mathrm{ps}/1^\circ \quad . \tag{4}$$

Therefore the calculated spatial distance $\Delta\mathrm{s}$ between the target and the TX antenna is equivalent to

$$\Delta\mathrm{s} = \frac{1}{2}\cdot\Delta\mathrm{t}\cdot\mathrm{c}_0\cdot\Delta\phi_{\mathrm{RX}} \approx 10\,\mathrm{cm} \tag{5}$$

with $\Delta\phi_{\mathrm{RX}} = 48^\circ$. The factor $\frac{1}{2}$ accounts for the fact that the echo signal propagates to the target and back. Fig. 9 exemplarily shows the normalized cross-correlation energy of an incoming pulse with a template pulse that is time-shifted with $\mathrm{CLK_{RX}}$ phase variations in one-degree-steps which is equivalent to a spatial offset of 4.2 mm.

V. Conclusion

We have demonstrated a single band 3.1 - 10.6 GHz UWB pulse radar system. Experiments show a resolution capability of the system in the millimeter range. The system comprises two monopole antennas, two pulse generators, an LNA, two single-ended to differential converters, a four-quadrant Gilbert cell multiplier and an additional buffer amplifier to drive the $50\,\Omega$ measurement environment. All active devices have been designed and fabricated using a low cost $0.8\,\mu$m SiGe HBT technology. The inherent low system complexity and the high resolution capability make the system an ideal candidate for future high resolution short range radar systems.

Acknowledgment

The authors wish to thank ATMEL Germany GmbH Heilbronn for the excellent support. The work was financially supported by the DFG project UKoLoS.

References

[1] T. Wuchenauer, M. Nalezinski and W. Menzel, "Superregenerative incoherent UWB pulse radar system", *IEEE MTT-S Intern. Microwave Symp.*, June 11-16, 2006, San Francisco, USA, pp. 1410-1413.

[2] Y. Kawano et al., "An RF chipset for impulse radio UWB using $0.13\,\mu$m InP-HEMT technology", *IEEE MTT-S Intern. Microwave Symp.*, June 11-16, 2006, San Francisco, USA, pp. 316-319.

[3] J. Sachs, P. Peyerl, M. Kmec and F. Tkac, "Digital ultra-wideband-sensor electronics integrated in SiGe-technology", *Proceedings of the EuMC*, vol. 2, pp. 539-542, September 2002.

[4] Federal Communications Commission: Revision of part 15 of the commission's rule regarding ultra-wideband transmission systems, First Report and Order, ET Docket 98-153, FCC 02-48, pp. 1-118, 2002.

[5] A. Schüppen et al., "An 80 GHz SiGe production technology", *III-V Review*, vol. 14, pp. 42-46, August 2001.

[6] H. Sheng, P. Orlik, A. M. Haimovich, L. J. Cimini and J. Zhang, "On the spectral and power requirements for ultra-wideband transmission", *IEEE Conf. on Communications*, Anchorage, USA, 11-15 May, 2003, pp. 738-742.

[7] H. Kim and Y. Joo, "Fifth-derivative Gaussian pulse generator for UWB system", *IEEE Radio Frequency Integrated Circuits (RFIC) Symp.*, Long Beach, USA, 12-14 June, 2005, pp. 671-674.

[8] J. Dederer, A. Trasser and H. Schumacher, "SiGe impulse generator for single-band ultra-wideband applications", *International SiGe Technology and Device Meeting*, Princeton, USA, 15-17 May, 2006, pp. 274-275.

[9] J. Jung, W. Choi and J. Choi, "A small wideband microstrip-fed monopole antenna", *Microwave and Wireless Components Lett.*, vol. 15, no. 10, pp. 703-705, October 2005.

[10] J. Dederer, A. Trasser and H. Schumacher, "Compact SiGe HBT low noise amplifiers for 3.1-10.6 GHz ultra-wideband applications", *Topical Meeting on Silicon Monolithic Integrated Circuits in RF Systems*, San Diego, USA, 18-20 Jan, 2006, pp. 391-394.